Journal of Multidisciplinary and Translational Research (JMTR)

journal homepage: https://journals.kln.ac.lk/jmtr/

Synthesis, crystal structure, luminescence properties, silica nanoparticle encapsulation, and antimicrobial activity of an Eu(III) β-diketonate complex with 4,7-dimethyl-1,10-phenanthroline

A.G.N.D. Darsanasiri[1], Louis C. Martin[1], Kristy M. Rogers[1], Gayanthi Attanayake[1], Indrani Bose[2], Christian F. Gainer[3], Robert D. Pike[4], Marek Romanowski[3], and Channa R. De Silva[1]*

[1]*Department of Chemistry and Physics, Western Carolina University, Cullowhee, NC, 28723, USA*
[2]*Department of Biology, Western Carolina University, Cullowhee, NC, 28723, USA*
[3]*Biomedical Engineering, Bio5 Institute, University of Arizona, Tucson, AZ, 85721, USA*
[4]*Department of Chemistry, College of William and Mary, Williamsburg, VA, 23187, USA*

Abstract

A novel luminescent europium(III) β-diketonate complex, $Eu(btfa)_3(dmphen)$ [btfa = 4,4,4-trifluoro-1-phenyl-1,3-butanedione; dmphen = 4,7-dimethyl-1,10-phenanthroline], was synthesized and investigated as a potential multifunctional material for optical and biological applications. The complex was prepared from the precursor $Eu(btfa)_3(H_2O)_2$ and structurally characterized by single-crystal X-ray diffraction. Crystallographic analysis revealed an eight-coordinate Eu(III) center adopting a distorted square-antiprismatic geometry, coordinated by six oxygen atoms from three btfa ligands and two nitrogen atoms from a chelating dmphen ligand. Photophysical studies showed that the complex exhibits intense Eu(III)-centered red emission dominated by the hypersensitive $^5D_0 \rightarrow {}^7F_2$ transition at 614 nm. Replacement of coordinated water molecules with the dmphen ligand significantly enhanced the luminescence performance, resulting in a quantum yield of 21% and a luminescence lifetime of 0.813 ms in dichloromethane solution, compared with 7.5% and 0.470 ms, respectively, for the precursor aqua complex. To improve aqueous dispersibility and potential biocompatibility, $Eu(btfa)_3(dmphen)$ was incorporated into silica nanoparticles using a modified Stöber sol–gel process. The resulting nanoparticles exhibited spherical morphology with average diameters of approximately 40–45 nm and remained well dispersed in water without visible aggregation. The silica-encapsulated materials retained the characteristic Eu(III) emission at 614 nm, with luminescence quantum yields dependent on complex loading, reaching a maximum value of 11.58% for nanoparticles prepared with 40 mg of $Eu(btfa)_3(dmphen)$. Antimicrobial studies performed against *Escherichia coli*, *Staphylococcus epidermidis*, and *Staphylococcus aureus* demonstrated that $Eu(btfa)_3(dmphen)$ exhibited substantially higher antibacterial activity than the precursor complex and starting materials. The enhanced activity is attributed to the incorporation of the hydrophobic dmphen ligand, which may facilitate cellular uptake and interactions with intracellular biomolecular targets. These results demonstrate that $Eu(btfa)_3(dmphen)$ and its silica nanoparticle formulations are promising candidates for luminescent bioimaging and antimicrobial applications.

Keywords: Europium(III) complex, β-diketonate, luminescence, silica nanoparticles, antimicrobial activity, lanthanide photophysics

Article info

Article history:
Received 28th March 2026
Received in revised form 30th April 2026
Accepted 20th June 2026
Available online 30th June 2026

ISSN (E-Copy): ISSN 3051-5262
ISSN (Hard copy): ISSN 3051-5602
Doi: https://doi.org/10.4038/jmtr.v11i1.432
ORCID iD: https://orcid.org/0000-0002-2029-3483
*Corresponding author:
E-mail address: mhdesilva@email.wcu.edu
(Channa R. De Silva)

Introduction

Extensive research has been conducted on lanthanide β-diketonate complexes because of their promising applications in display devices, luminescent sensors, biomedical imaging, tunable lasers, and optical amplifiers (De Silva et al., 2007; Tessitore et al., 2023). Among these complexes, europium (Eu)-based β-diketonates have attracted particular attention for biological applications owing to their intense red emission at 614 nm and their relatively long luminescence lifetimes (Dalal et al., 2023). These complexes exhibit distinctive photophysical properties, including sharp and well-resolved emission bands, high photostability with minimal photobleaching, and large Stokes shifts, making them highly advantageous for luminescence-based applications.

A typical Eu(III) β-diketonate complex comprises three anionic oxygen-donor β-diketonate ligands and a neutral bi- or tridentate nitrogen-donor ligand, which together provide a saturated coordination environment around the metal center (De Silva et al., 2007). The choice of ligands is critical because the direct excitation of the Eu(III) ion through *f–f* electronic transitions is Laporte-forbidden, resulting in weak absorption and low luminescence efficiency (Görller-Walrand & Binnemans, 1998). In contrast, the coordinated ligands possess high molar absorption coefficients and serve as efficient light-harvesting antennas, thereby enhancing the luminescence quantum yield of the complex.

Upon photoexcitation, the ligands are initially promoted to their excited singlet states, followed by intersystem crossing to the corresponding triplet states. Subsequently, energy is transferred from the ligand-centered triplet states to the excited states of the Eu(III) ion, ultimately leading to characteristic metal-centered luminescence. Thus, europium emission arises primarily through a ligand-to-metal energy transfer process, commonly referred to as the antenna effect (Junker et al., 2018).

Importantly, ligand modification can be achieved without significantly altering the emission wavelength because the 4*f* electrons of the Eu(III) ion are effectively shielded from the surrounding ligand field. As a result, changes in ligand structure have minimal influence on the intrinsic electronic transitions of the metal ion. Such modifications are therefore primarily employed to tune the photophysical properties and optimize the processability of Eu(III) complexes for a wide range of optical and photonic applications.

Efficient ligand-to-metal energy transfer requires careful matching of the ligand-centered singlet and triplet excited-state energies with the excited states of the Eu(III) ion. A variety of β-diketonate ligands have been employed as sensitizers for Eu(III), including thenoyltrifluoroacetone (tta), 4,4,4-trifluoro-1-phenyl-1,3-butanedione (btfa), and acylpyrazole derivatives, many of which afford high luminescence quantum yields (Dalal et al., 2023; De Silva et al., 2007).

In addition to variations in the β-diketonate ligand framework, neutral nitrogen-donor ligands play a crucial role in completing the coordination sphere of the metal ion by replacing coordinated water molecules present in precursor complexes such as Eu(β-diketonate)$_3$(H_2O)$_2$. The incorporation of neutral ligands reduces non-radiative deactivation arising from O–H vibrational oscillators, thereby enhancing Eu(III)-centered luminescence (Galaup et al., 2002). Furthermore,

these ligands may contribute to light absorption and participate in the sensitization process through energy transfer to the metal center. Consequently, the design and modification of neutral nitrogen-donor ligands have become important areas of research in lanthanide photophysics. Numerous structural modifications of the widely used 2,2′-bipyridine and 1,10-phenanthroline ligands have been reported (Campello et al., 2019). For example, extension of the phenanthroline π-conjugated framework has led to fused aromatic systems such as azatriphenylene and phenazine derivatives, which serve as effective neutral ligands in Eu(III) β-diketonate complexes (Santra et al., 2018).

Our research has focused on the development of novel luminescent Eu(III) complexes incorporating bipyridine- and phenanthroline-based nitrogen-donor ligands. In particular, we successfully synthesized and structurally characterized several Eu(III) β-diketonate complexes containing 4,4′-dimethoxy-2,2′-bipyridine and 4,7-dimethyl-1,10-phenanthroline through single-crystal X-ray diffraction studies (De Silva et al., 2007). These investigations demonstrated that methoxy and methyl substitution of the nitrogen-donor ligands can significantly enhance luminescence efficiency, with the extent of enhancement being strongly dependent on the coordination environment surrounding the Eu(III) center.

The photobleaching and quenching of organic dyes, together with the toxicity concerns associated with quantum dots, have significantly limited their applications in biological imaging, particularly for *in vivo* studies. As an alternative, highly luminescent europium complexes dispersed within silica nanoparticles have emerged as promising probes for biomedical imaging applications (Tan et al., 2004). Only a limited number of studies have reported the synthesis and characterization of lanthanide-based complexes with potential bio-imaging capabilities.

However, further improvements in both biocompatibility and luminescence efficiency are required before these materials can be widely adopted for *in vivo* imaging applications. Recently, Wang and co-workers reported the synthesis of two-photon-responsive lanthanide chromophores embedded in silica nanoparticles prepared via a microemulsion-based solution process for cellular imaging (Ma et al., 2025). They demonstrated a convenient one-step strategy for stabilizing lanthanide complexes in aqueous media through encapsulation within silica nanoparticles. In this approach, the lanthanide complexes were successfully grafted onto the silica nanoparticle surface.

Despite the extensive interest in lanthanide β-diketonate complexes for luminescent applications, investigations into their biological properties, particularly antimicrobial and anticancer activities, remain relatively limited. Nevertheless, recent studies have demonstrated the potential of lanthanide complexes as antimicrobial agents, including several systems incorporating phenanthroline-based neutral ligands (Gao et al., 2021). For example, the antimicrobial activities of Er(III), Tb(III), Dy(III), and Ho(III) complexes containing 3-bromo-5-iodobenzoate and 1,10-phenanthroline ligands have been evaluated against *E. coli* (Liu et al., 2013). These complexes exhibited moderate antimicrobial activity against both *Candida albicans* and *S. aureus*. Similarly, a series of lanthanide complexes with the general formula $[Ln(DmeoxBA)_3(phen)]_2$ [Ln = Tb, Dy, Er, and Yb; DmeoxBA = 3,5-dimethoxybenzoate; phen = 1,10-phenanthroline] was investigated against the same bacterial and fungal species.

The results revealed metal-dependent antimicrobial behavior: the Tb(III) and Dy(III) complexes showed activity against *E. coli*, whereas the Er(III) and Yb(III) analogues were effective against *C. albicans*.

Lanthanide complexes containing modified phenanthroline derivatives have also attracted attention as potential antimicrobial agents. For instance, Eu(III) and Yb(III) β-diketonate complexes incorporating 1,10-phenanthroline-5,6-dione as the neutral ligand have been reported to exhibit notable antimicrobial activity against *Proteus penneri*. The observed activity was attributed to the presence of the quinonoid functional group, whose redox properties are believed to disrupt bacterial cellular processes and interfere with essential enzymatic functions, ultimately leading to microbial cell death.

In the present study, a novel Eu(III) β-diketonate complex containing 4,4,4-trifluoro-1-phenyl-1,3-butanedione and 4,7-dimethyl-1,10-phenanthroline ligands was synthesized and characterized. The structural and photophysical properties of the complex were investigated using single-crystal X-ray diffraction, UV–visible absorption spectroscopy, and luminescence spectroscopy. A sol–gel-based synthetic approach was subsequently developed to incorporate the Eu(III) complex into silica nanoparticles. Furthermore, the antimicrobial activity of the complex was evaluated against *E. coli*, *S. epidermidis*, and *S. aureus*, thereby assessing its potential for biological applications in addition to its luminescent properties.

Methodology

Europium(III) chloride hexahydrate ($EuCl_3 \cdot 6H_2O$), 4,4,4-trifluoro-1-phenyl-1,3-butanedione (Hbtfa), 4,7-dimethyl-1,10-phenanthroline (dmphen), and Tryptic Soy Agar were procured from Fisher Scientific Inc. and used without further purification. Bacterial strains of *E. coli, S. aureus*, and *S. epidermidis* were obtained from Ward's Science (USA) and employed in the antimicrobial assays. All chemicals and solvents were of analytical-reagent grade and were used without further purification unless otherwise noted. UV–visible absorption spectra were recorded on an Agilent 8453 UV–visible spectrophotometer using dichloromethane as the solvent. Luminescence measurements were carried out using a PerkinElmer LS-55 fluorescence spectrometer equipped with a 5 nm slit width and quartz cuvettes.

Emission in the visible region was generated by excitation with a xenon arc lamp and detected using a photomultiplier tube positioned at 90° relative to the incident beam. Samples were excited at 340 nm, and the emission spectra were recorded over the wavelength range of 400–700 nm at a scan rate of 200 nm min^{-1}.

Photoluminescence quantum yields were determined using cresyl violet perchlorate in methanol as the reference standard, for which a quantum yield (Φ) of 0.54 has been reported. Relative quantum yields were calculated using the following equation (De Silva et al., 2007).

$$\phi_S = \phi_R \, (Abs_R / Abs_S) \, (A_S / A_R) \, (n^2_S / n^2_R)$$

In the above equation, Abs, A, and n represent the absorbance at the wavelength of maximum absorption, the integrated emission intensity (area under the emission spectrum), and the

refractive index of the solvent, respectively. The subscripts R and S denote the reference and sample, respectively.

Single crystals suitable for X-ray diffraction analysis were obtained by the slow evaporation of saturated solutions of the $Eu(btfa)_3(dmphen)$ complex in an ethanol/acetone (1:1, v/v) solvent mixture at room temperature. Details of the X-ray data collection procedures and crystallographic structure refinements are summarized in Table 1.

Table 1: Crystal data and structure refinement for $Eu(btfa)_3$dmphen complex

Parameter	**Value**
Empirical formula	$C_{44}H_{30}EuF_9N_2O_6$
Formula weight	1005.66
Temperature	100(2) K
Wavelength	1.54178 Å
Crystal system	Monoclinic
Space group	C2/c
Unit cell dimensions	a = 36.6051(10) Å a= 90°. b = 10.8940(3) Å b= 111.9080(10)°. c = 22.2613(6) Å g = 90°.
Volume	8236.2(4) $Å^3$
Z	8
Density (calculated)	1.622 mg/m^3
Absorption coefficient	11.717 mm^{-1}
F(000)	4000
Crystal size	0.45 x 0.29 x 0.20 mm^3
Theta range for data collection	2.60 to 66.97°.
Index ranges	-43<=h<=43, -10<=k<=12, -26<=l<=26
Reflections collected	44146
Independent reflections	7190 [R(int) = 0.0590]
Completeness to theta = 66.97°	98.1 %
Absorption correction	Numerical
Max. and min. transmission	0.1985 and 0.0770
Refinement method	Full-matrix least-squares on F^2
Data / restraints / parameters	7190 / 0 / 561
Goodness-of-fit on F^2	1.031
Final R indices [I>2sigma(I)]	R1 = 0.0401, wR2 = 0.1015
R indices (all data)	R1 = 0.0432, wR2 = 0.1039
Largest diff. peak and hole	1.255 and -0.802 $e.Å^{-3}$

Luminescence lifetime measurements of the complexes, both in the solid state (as dry powders) and in dichloromethane solution, were performed using a Hamamatsu R928 photomultiplier tube coupled to a 500 MHz digital storage oscilloscope (Tektronix TDS 620B). Excitation was provided

by a tunable optical parametric oscillator (OPO) pumped by a Q-switched Nd:YAG laser operating at a repetition rate of 20 Hz and delivering pulses with a width of 3 ns.

Synthesis of $Eu(btfa)_3(H_2O)_2$ complex

Hbtfa (3.0 mmol, 648 mg) was dissolved in water (15 mL), and NaOH (3.0 mmol, 120 mg) was added with stirring. The resulting mixture was stirred until a clear solution was obtained. A solution of $EuCl_3 \cdot 6H_2O$ (1.0 mmol, 366 mg) in nanopure water (15 mL) was then added dropwise to the Hbtfa/NaOH solution, and the reaction mixture was maintained at 60 °C with continuous stirring for 30 min. Subsequently, the mixture was allowed to stir at room temperature for an additional 2.5 h. The resulting precipitate was collected by vacuum filtration, washed thoroughly with water (500 mL), and dried in air to afford $Eu(btfa)_3(H_2O)_2$ (Figure 1).

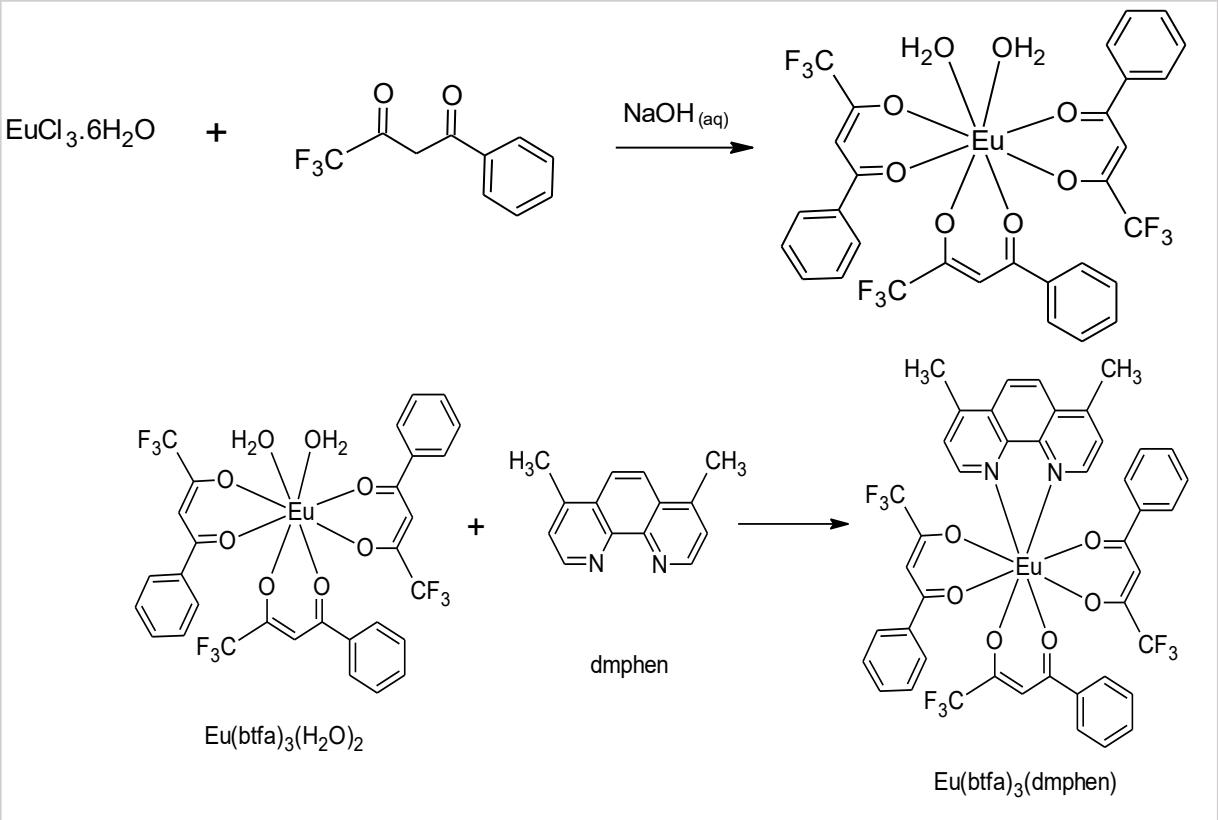

Figure 1. Synthesis of Eu(btfa)3(dmphen) complex

Synthesis of $Eu(btfa)_3$(dmphen) complex

$Eu(btfa)_3(H_2O)_2$ (0.10 mmol, 83.3 mg) was dissolved in acetone (approximately 15 mL). To this solution was added a solution of 4,7-dimethyl-1,10-phenanthroline (dmphen) (0.10 mmol, 22.6 mg) in acetone (15 mL). The reaction mixture was heated at 45 °C with stirring for 30 min and subsequently stirred at room temperature for 24 h. The resulting mixture was filtered to remove any insoluble impurities, and the filtrate was allowed to evaporate slowly at room temperature. Pale yellow crystalline solids suitable for analysis were obtained and isolated as the analytically pure product.

Determination of antimicrobial activity

Antimicrobial activity was evaluated against the Gram-positive bacteria *S. epidermidis* and *S. aureus* and the Gram-negative bacterium *E. coli* using a modified agar disc diffusion method and the minimum inhibitory concentration (MIC) method. Bacterial cultures were grown on Tryptic Soy Agar at 37 °C for 24 h. Subsequently, 4–5 well-isolated colonies were selected, and the bacterial suspension was prepared and adjusted to an optical density (OD) of 0.3. An aliquot (100 µL) of the cell suspension was evenly spread onto Mueller–Hinton agar plates. Sterile filter paper discs (10 mm diameter), pre-soaked with the test solutions, were then placed aseptically and at equal distances on the inoculated agar surface. The discs were impregnated with 0.25 M solutions of $Eu(btfa)_3(dmphen)$, $Eu(btfa)_3(H_2O)_2$, $EuCl_3{\cdot}6H_2O$, dmphen, and Hbtfa prepared in dimethylformamide (DMF). The inoculated plates were incubated at 37 °C for 24 h, after which the antimicrobial activity was assessed by measuring the diameter of the zone of inhibition surrounding each disc. In each case, the diameter of the innermost clear zone of growth inhibition was recorded.

The minimum inhibitory concentration test was carried out using a broth microdilution method in 96-well microplates. Tryptic Soy Agar (TSA) broth (50 µL) was added to each well of a sterile 96-well plate. Two-fold serial dilutions of the compounds in DMF were prepared across the wells by transferring 50 µL from the first well to the subsequent well and repeating the dilution process sequentially up to well 10. A bacterial suspension (25 µL) was then inoculated into wells 1–10, while wells 11 and 12 served as control wells. Alamar Blue reagent (25 µL) was added to all wells except well 12, which was designated as the negative control.

The microplates were incubated at 37 °C for 24–48 h. Following incubation, bacterial growth was assessed visually based on the color change of the Alamar Blue indicator. The MIC was defined as the lowest compound concentration that completely inhibited visible bacterial growth, indicated by the retention of the original blue color of the dye. Wells remaining blue were considered to contain no viable bacterial cells, whereas wells exhibiting a pink color indicated metabolically active and viable bacterial populations. Thus, the transition from blue to pink served as an indicator of bacterial growth and cellular respiration.

Synthesis of Eu(btfa)3(dmphen) incorporated silica nanoparticles

$Eu(btfa)_3(dmphen)$-incorporated silica nanoparticles were prepared via a modified Stöber process (Singla et al., 2009). Particle size was controlled by optimizing the reaction conditions and varying the concentration of the encapsulated Eu(III) complex. The $Eu(btfa)_3(dmphen)$ complex (20 mg, 0.0336 mmol; 30 mg, 0.050 mmol; or 40 mg, 0.067 mmol) was dissolved in ethanol (50 mL), and the resulting mixture was stirred at 30 °C for 30 min to ensure complete dispersion of the complex. Subsequently, tetraethyl orthosilicate (TEOS, 3 mL, 0.0133 mol), 28% aqueous NH_4OH solution (1 mL), and nanopure water (2 mL) were added to the $Eu(btfa)_3(dmphen)$/ethanol mixture. The reaction mixture was then stirred at 55 °C for 18 h to promote hydrolysis and condensation of TEOS, leading to the formation of silica nanoparticles encapsulating the Eu(III) complex (Figure 2).

Upon completion of the reaction, the nanoparticle suspension was centrifuged at 4000 rpm for 20 min to isolate the Eu(III) complex-incorporated silica particles. The resulting pellets were washed several times with ethanol to remove residual reactants and unreacted species, followed by centrifugation at 4000 rpm for 20 min after each washing step. The purified $Eu(btfa)_3(dmphen)$-incorporated silica nanoparticles were then collected for further characterization and photophysical studies.

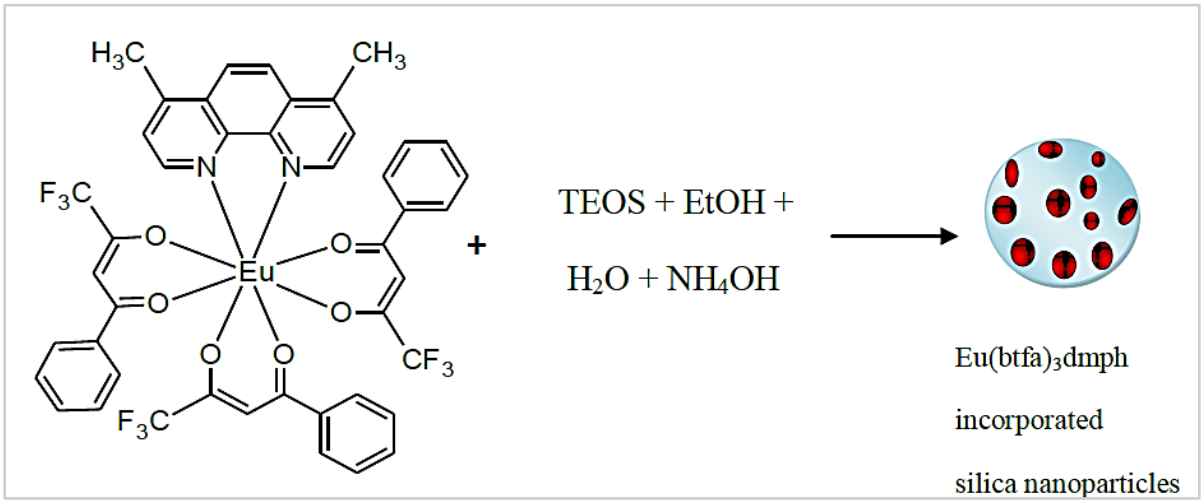

Figure 2. Eu(btfa)3(dmphen) complex-incorporated silica nanoparticles

Scanning electron microscopy studies

The morphology and particle size of the $Eu(btfa)_3(dmphen)$-incorporated silica nanoparticles were examined using scanning transmission electron microscopy (STEM) on a Hitachi HD-2000 instrument operated at an accelerating voltage of 200 kV. Samples were prepared by dispersing the nanoparticles in water at a concentration of 1 $mg.mL^{-1}$. An aliquot (200 µL) of each dispersion was deposited onto a carbon-coated copper grid (300 mesh) and allowed to dry at room temperature for 4 h prior to analysis.

Results

Synthesis and X-ray crystallography

$Eu(btfa)_3(H_2O)_2$ was initially synthesized using a 3:1 molar ratio of $EuCl_3 \cdot 6H_2O$ to Hbtfa. Sodium hydroxide was employed to deprotonate the acidic α-proton of Hbtfa, facilitating coordination of the resulting $btfa^-$ ligands to the Eu(III) center. Three anionic btfa ligands coordinate to Eu(III) to form the neutral precursor complex $Eu(btfa)_3(H_2O)_2$. Subsequent substitution of the coordinated water molecules with the nitrogen-donor ligand 2,9-dimethyl-1,10-phenanthroline (dmphen) afforded the coordinatively saturated complex $Eu(btfa)_3(dmphen)$.

The molecular structure of $Eu(btfa)_3(dmphen)$, as determined by single-crystal X-ray diffraction, is shown in Figure 3a. The Eu(III) ion is eight-coordinate, with the coordination sphere comprising six oxygen atoms from three btfa ligands and two nitrogen atoms from a chelating dmphen ligand. The coordination geometry around the Eu(III) center is best described as a distorted square antiprism.

Selected bond distances and bond angles are summarized in Table 2. The average Eu–O and Eu–N bond distances are 2.362 and 2.584 Å, respectively. The average Eu–N bond distance in $Eu(btfa)_3(dmphen)$ is comparable to that reported for the related complex $Eu(tta)_3(dmphen)$ (2.581 Å). However, it is slightly shorter than the corresponding distance observed in $Eu(hfa)_3(dmphen)(EtOH)$ (2.594 Å). Variations in Eu–N bond lengths are likely influenced by both the electronic properties of the coordinated β-diketonate ligands and the steric effects imposed by the ligand environment surrounding the metal center (De Silva et al., 2007).

The crystal packing diagram of $Eu(btfa)_3(dmphen)$ is presented in Figure 3b. Intermolecular aromatic π–π stacking interactions involving coordinated dmphen ligands are evident within the crystal lattice. The planar nature of the dmphen ligand promotes these π–π interactions, which contribute significantly to the stabilization and packing arrangement of the molecules in the solid state.

In addition, weak intermolecular C–H···F hydrogen-bonding interactions are observed between fluorine atoms of the btfa ligands and methyl hydrogen atoms of neighboring dmphen ligands, further reinforcing the crystal packing structure.

Table 2: Selected bond lengths (Å) and angles (°) for Eu(btfa)3(dmphen) complex

Bond Lengths			
Bond	**Length (Å)**	**Bond**	**Length (Å)**
Eu(1)-O(3)	2.344(3)	Eu(1)-O(1)	2.384(2)
Eu(1)-O(6)	2.344(3)	Eu(1)-O(4)	2.388(3)
Eu(1)-O(5)	2.348(3)	Eu(1)-N(1)	2.560(4)
Eu(1)-O(2)	2.365(3)	Eu(1)-N(2)	2.607(3)
Bond Angles			
Atoms	**Angle (°)**	**Atoms**	**Angle (°)**
O(3)-Eu(1)-O(6)	80.64(10)	O(1)-Eu(1)-O(4)	144.41(9)
O(3)-Eu(1)-O(5)	140.75(10)	O(3)-Eu(1)-N(1)	109.49(10)
O(6)-Eu(1)-O(5)	73.40(12)	O(6)-Eu(1)-N(1)	145.82(11)
O(3)-Eu(1)-O(2)	78.28(9)	O(5)-Eu(1)-N(1)	79.58(12)
O(6)-Eu(1)-O(2)	75.55(10)	O(2)-Eu(1)-N(1)	137.73(10)
O(5)-Eu(1)-O(2)	121.31(11)	O(1)-Eu(1)-N(1)	80.08(9)
O(3)-Eu(1)-O(1)	141.38(9)	O(4)-Eu(1)-N(1)	73.75(10)
O(6)-Eu(1)-O(1)	112.89(10)	O(3)-Eu(1)-N(2)	78.48(9)
O(5)-Eu(1)-O(1)	76.97(10)	O(6)-Eu(1)-N(2)	150.03(10)
O(2)-Eu(1)-O(1)	71.20(9)	O(5)-Eu(1)-N(2)	134.94(11)
O(3)-Eu(1)-O(4)	71.62(9)	O(2)-Eu(1)-N(2)	79.32(9)
O(6)-Eu(1)-O(4)	79.25(10)	O(1)-Eu(1)-N(2)	73.15(9)
O(5)-Eu(1)-O(4)	74.95(10)	O(4)-Eu(1)-N(2)	113.64(9)
O(2)-Eu(1)-O(4)	143.32(10)	N(1)-Eu(1)-N(2)	62.76(10)

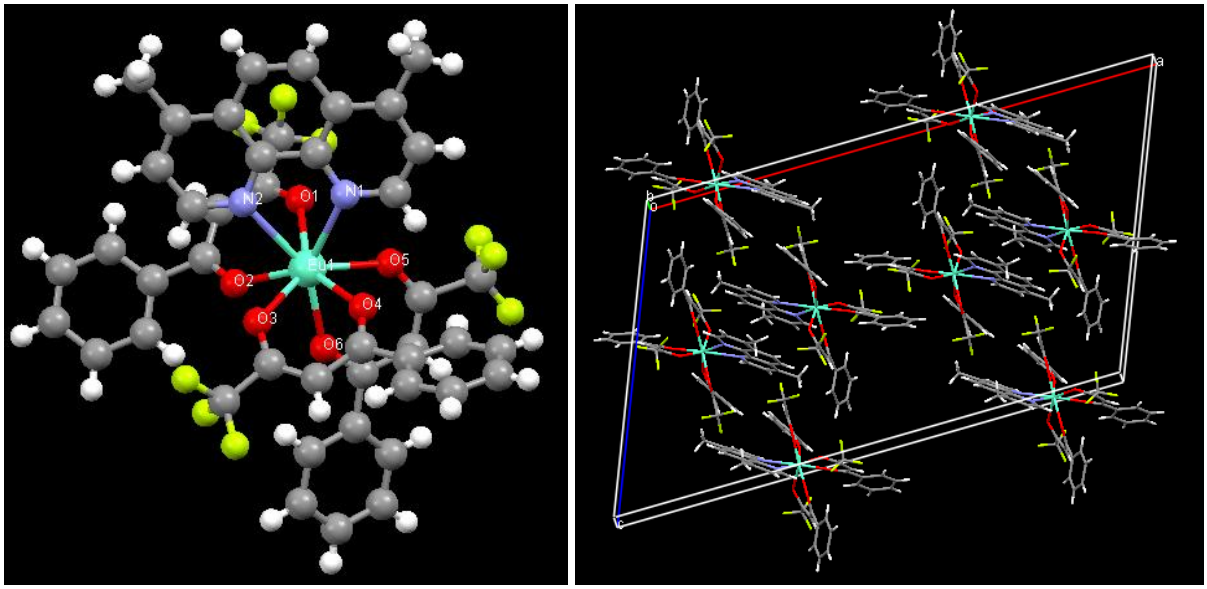

(a) **(b)**

Figure 3. (a) Single crystal X-ray crystal structure and (b) the unit cell packing diagram of Eu(btfa)3(dmphen) complex

Synthesis of nanoparticles and electron microscopy

$Eu(btfa)_3(dmphen)$-incorporated silica nanoparticles were successfully synthesized using a modified sol–gel method. Different loadings of the Eu(III) complex were investigated to evaluate their effect on nanoparticle formation and morphology. Scanning electron microscopy (SEM) images of the pristine silica nanoparticles and $Eu(btfa)_3(dmphen)$-incorporated silica nanoparticles are presented in Figure 4.

The unmodified silica nanoparticles exhibited a nearly spherical morphology with an average particle diameter of approximately 12 nm (Figure 4a). Incorporation of 20 mg of $Eu(btfa)_3(dmphen)$ resulted in an increase in particle size, yielding nanoparticles with an average diameter of approximately 45 nm (Figure 4b). For nanoparticles prepared with 30 mg and 40 mg of the Eu(III) complex, average particle diameters of approximately 40 nm were observed (Figure 4c and Figure 4d, respectively). The SEM images confirmed the successful formation of nanoparticles with relatively uniform size distributions and morphology following incorporation of the Eu(III) complex.

Furthermore, all $Eu(btfa)_3(dmphen)$-incorporated silica nanoparticles exhibited excellent dispersibility in water across the range of complex loadings investigated in this study. The nanoparticle suspensions remained homogeneous and produced optically clear dispersions without visible aggregation, indicating good colloidal stability in aqueous media.

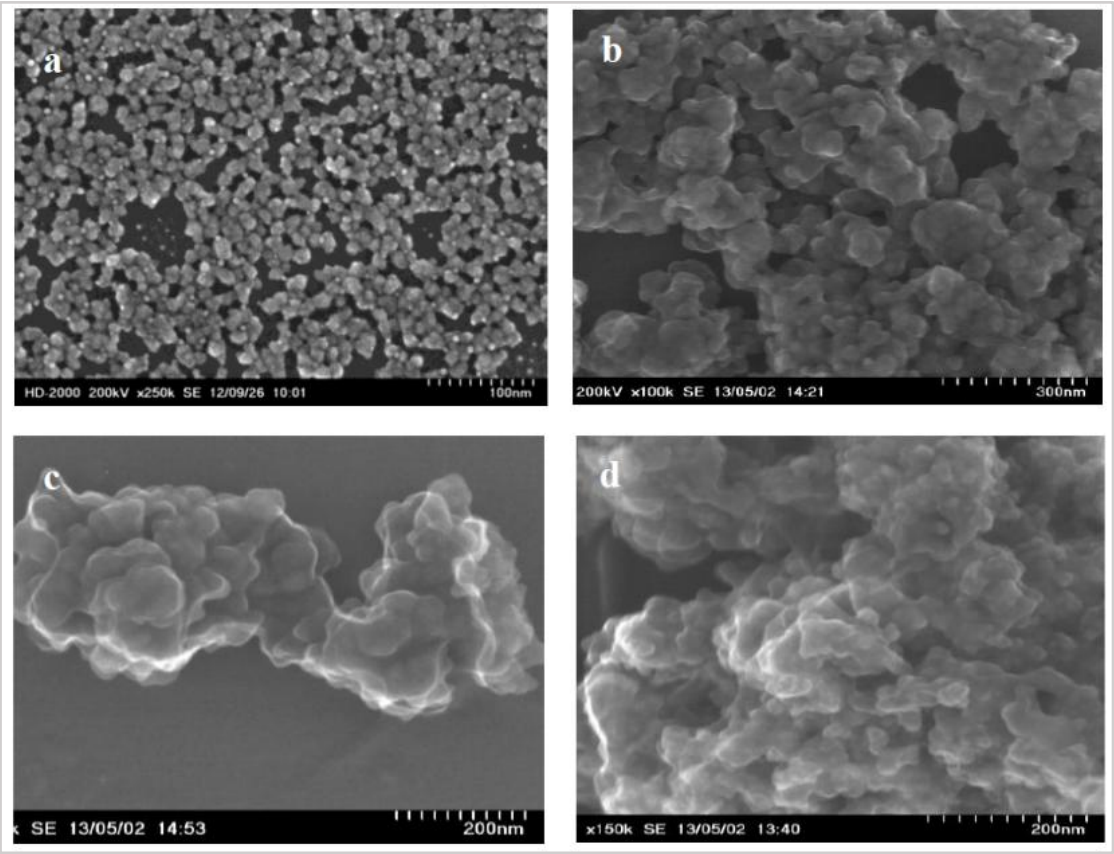

Figure 4. SEM image of (a) silica nanoparticles, (b) 20 mg of Eu(btfa)3dmph incorporated silica nanoparticles, (c) 30 mg of Eu(btfa)3dmph incorporated silica nanoparticles and (d) 40 mg of Eu(btfa)3(dmphen) incorporated silica nanoparticles prepared by using modified Stöber method

Photophysical studies

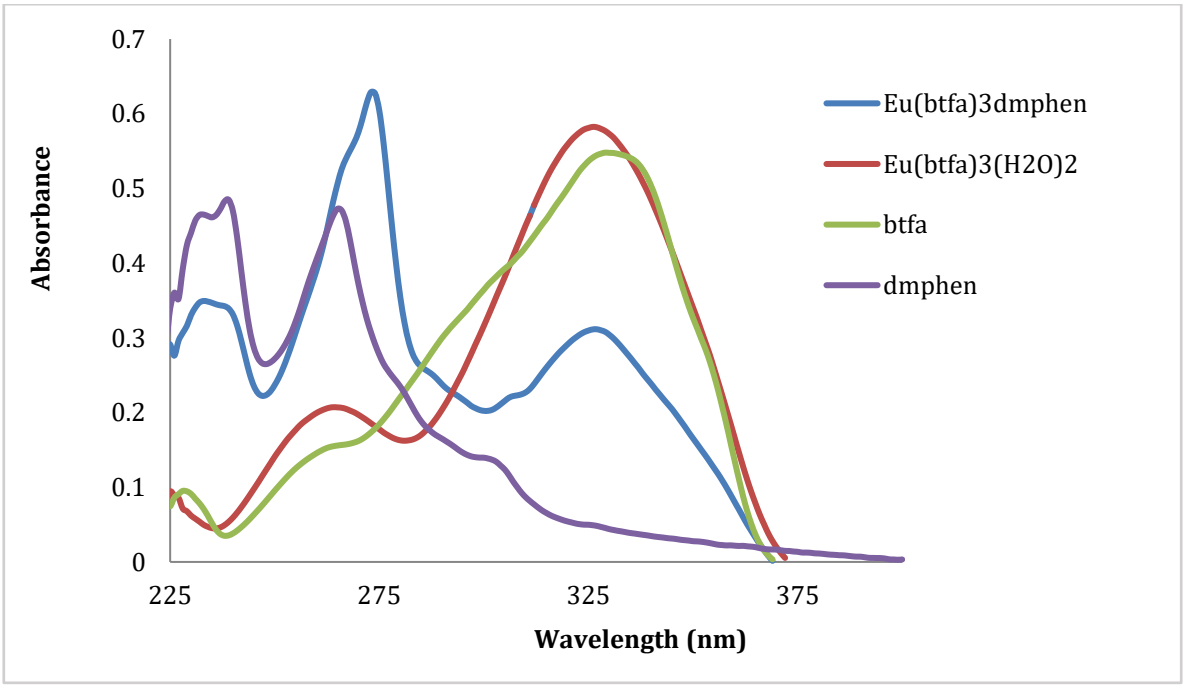

Figure 5. Absorption spectra of Eu(III) complexes and the corresponding ligands in dichloromethane

The UV–Vis absorption spectra of $Eu(btfa)_3(dmphen)$, $Eu(btfa)_3(H_2O)_2$, and the free ligands Hbtfa and dmphen are presented in Figure 5. The Hbtfa ligand exhibits characteristic absorption maxima at 260 and 330 nm. Similarly, the precursor complex $Eu(btfa)_3(H_2O)_2$ displays absorption bands at 264 and 326 nm, confirming the presence of coordinated btfa ligands. The nitrogen-donor ligand dmphen shows absorption maxima at 239 and 265 nm. The absorption spectrum of $Eu(btfa)_3(dmphen)$ exhibits prominent bands at 233, 273, and 327 nm, reflecting contributions from both the btfa and dmphen ligands. The absorption profiles of the complexes are primarily ligand-centered and are not significantly influenced by the Eu(III) ion. Consequently, light absorption occurs through the coordinated ligand framework, which subsequently transfers energy to the Eu(III) center.

As shown in Figure 6, a 1×10^{-6} M solution of $Eu(btfa)_3(dmphen)$ in dichloromethane exhibits intense red luminescence upon excitation at 350 nm. Both the btfa and dmphen ligands participate in the ligand-to-metal energy transfer process, resulting in characteristic Eu(III)-centered emission. The emission spectrum displays the typical Eu(III) transitions corresponding to $^5D_0 \rightarrow {}^7F_0$ (581 nm), $^5D_0 \rightarrow {}^7F_1$ (593 nm), $^5D_0 \rightarrow {}^7F_2$ (614 nm), and $^5D_0 \rightarrow {}^7F_3$ (654 nm). Among these transitions, the hypersensitive $^5D_0 \rightarrow {}^7F_2$ transition at 614 nm is the most intense, producing the characteristic bright red emission associated with Eu(III) complexes (Tan et al., 2004).

The luminescence intensity of $Eu(btfa)_3(dmphen)$ is significantly greater than that of $Eu(btfa)_3(H_2O)_2$. This enhancement can be attributed to the replacement of coordinated water molecules by the dmphen ligand. Coordinated H_2O molecules are known to promote non-radiative deactivation pathways through O–H vibrational oscillators, resulting in luminescence quenching (Nihonyanagi & Kanemitsu, 2004). In contrast, coordination of the rigid aromatic dmphen ligand reduces vibrational quenching and improves the efficiency of ligand-to-metal energy transfer, thereby enhancing the Eu(III) emission intensity.

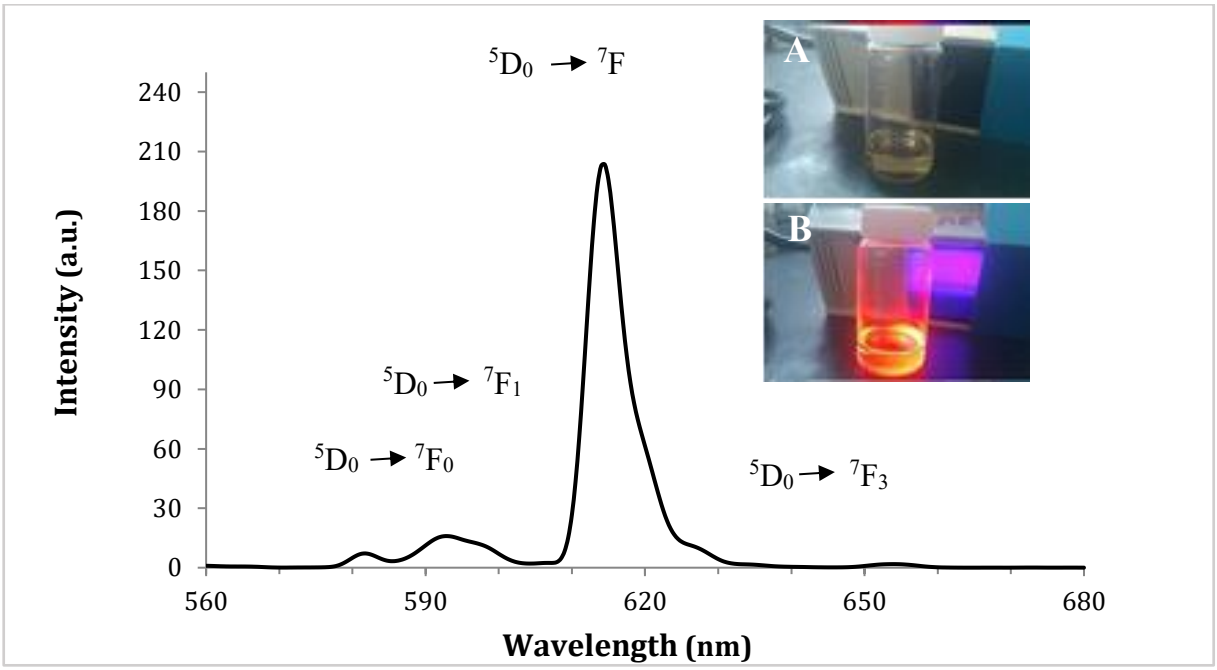

Figure 6. Luminescent spectrum of Eu(btfa)3dmphen in dichloromethane. Inset shows the complex before (A) and upon (B) UV excitation at 365 nm using a portable lamp.

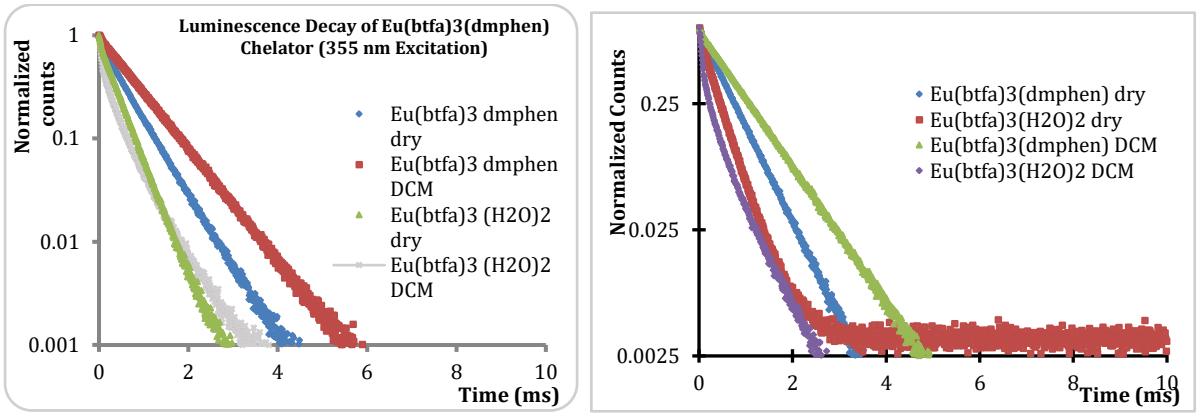

(a) **(b)**

Figure 7. Luminescent decay curves of **(a)** $Eu(btfa)_3dmphen$ and **(b)** $Eu(btfa)_3(H_2O)_2$ complexes upon 355 nm excitation (DCM=dichloromethane

The luminescence lifetimes of $Eu(btfa)_3(H_2O)_2$ and $Eu(btfa)_3(dmphen)$ were determined under both ligand-centered excitation (355 nm) and direct Eu(III) excitation (465 nm), using samples in the solid state and in dichloromethane solution. The luminescence decay profiles recorded at 355 nm excitation are presented in Figure 7. For $Eu(btfa)_3(dmphen)$ in the solid state, luminescence lifetimes of 0.593 and 0.572 ms were measured at excitation wavelengths of 355 and 465 nm, respectively. In dichloromethane solution, the corresponding lifetime values increased to 0.813 and 0.811 ms. In contrast, the precursor complex $Eu(btfa)_3(H_2O)_2$ exhibited significantly shorter lifetimes. In the solid state, lifetimes of 0.384 and 0.371 ms were observed at 355 and 465 nm excitation, respectively, whereas in dichloromethane solution lifetimes of 0.470 and 0.474 ms were obtained.

The longer luminescence lifetimes observed for $Eu(btfa)_3(dmphen)$ relative to $Eu(btfa)_3(H_2O)_2$ can be attributed to the absence of coordinated water molecules in the former complex. Coordinated H_2O ligands are known to facilitate non-radiative deactivation through O–H vibrational oscillators, resulting in efficient quenching of Eu(III)-centered emission. Consequently, the presence of coordinated water molecules in $Eu(btfa)_3(H_2O)_2$ increases non-radiative decay pathways and shortens the luminescence lifetime. In contrast, substitution of the aqua ligands by the chelating dmphen ligand yields a coordinatively saturated environment around the Eu(III) ion, thereby minimizing O–H vibrational coupling and suppressing non-radiative relaxation processes.

Notably, direct excitation of the Eu(III) ion at 465 nm through *f–f* electronic transitions did not substantially alter the measured lifetimes relative to those obtained under ligand excitation at 355 nm. This observation suggests that the intrinsic excited-state decay processes of Eu(III) remain largely unchanged regardless of the excitation pathway. Therefore, the shorter lifetimes observed for $Eu(btfa)_3(H_2O)_2$ are primarily attributable to vibrational quenching by coordinated water molecules rather than differences in energy-transfer efficiency between the ligand and metal center. The relatively long luminescence lifetime of $Eu(btfa)_3(dmphen)$ highlights its potential utility in time-resolved bioimaging applications, where extended emission lifetimes enable efficient rejection of short-lived background fluorescence and improved signal-to-noise ratios.

The luminescence quantum yields of $Eu(btfa)_3(dmphen)$ and $Eu(btfa)_3(H_2O)_2$ were calculated to be 21% and 7.5%, respectively. As expected, the dmphen-containing complex exhibits a substantially higher quantum yield than its aqua analogue. The enhanced luminescence efficiency of $Eu(btfa)_3(dmphen)$ can be attributed to two key factors. First, the absence of coordinated O–H oscillators significantly reduces non-radiative quenching pathways. Second, the coordinated dmphen ligand functions as an efficient light-harvesting antenna, absorbing ultraviolet radiation through $\pi \rightarrow \pi^*$ electronic transitions and subsequently transferring the absorbed energy to the Eu(III) center. The combined effects of reduced non-radiative decay and improved sensitization of the Eu(III) ion contribute to the markedly higher quantum yield observed for $Eu(btfa)_3(dmphen)$.

$Eu(btfa)_3(dmphen)$-incorporated silica nanoparticles also exhibited Eu(III)-centered luminescence at 614 nm upon UV excitation (Figure 8). The luminescence quantum yields of the $Eu(btfa)_3(dmphen)$-incorporated silica nanoparticles were found to depend strongly on the loading of the Eu(III) complex within the silica matrix. The nanoparticles prepared with 30 mg of $Eu(btfa)_3(dmphen)$ exhibited a luminescence quantum yield of 3.1%, whereas those prepared with 40 mg of the complex showed a substantially higher quantum yield of 11.58%.

These results indicate that the luminescence efficiency of the nanoparticles is influenced by the amount of $Eu(btfa)_3(dmphen)$ encapsulated within the silica network. An increase in the lanthanide complex loading resulted in enhanced emission efficiency, suggesting more effective light harvesting and energy transfer within the nanoparticle system. The higher quantum yield observed for the 40 mg sample may be attributed to the greater concentration of luminescent Eu(III) centers embedded in the silica matrix, thereby increasing the overall emission intensity.

Although encapsulation within silica provides protection against environmental quenching and improves the stability of the luminescent complex, the quantum yields of the nanoparticle systems remain lower than that of the free $Eu(btfa)_3(dmphen)$ complex. This reduction may arise from partial attenuation of excitation and emission processes by the silica matrix, as well as additional non-radiative deactivation pathways associated with the nanoparticle environment. Nevertheless, the observed increase in quantum yield with increasing Eu(III) complex loading demonstrates that the luminescent properties of the silica nanoparticles can be effectively tuned by controlling the amount of $Eu(btfa)_3(dmphen)$ incorporated during synthesis.

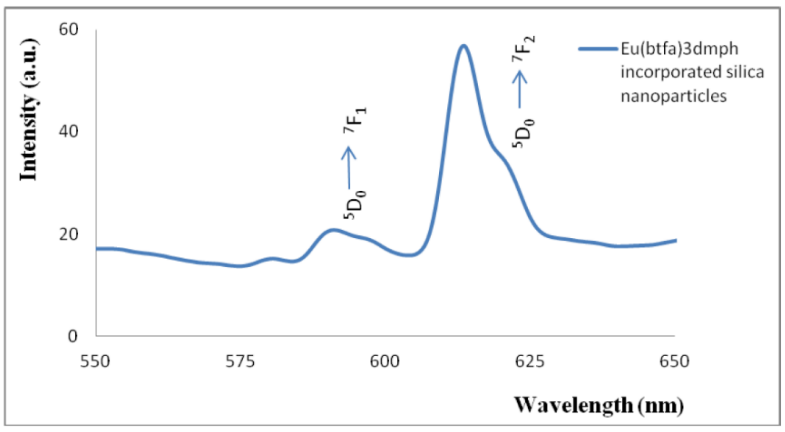

Figure 8. Luminescence spectrum of $Eu(btfa)_3$dmphen-incorporated silica nanoparticles dispersed in water (excitation wavelength = 350 nm).

Antimicrobial studies
Agar diffusion method

The antimicrobial activities of the two Eu(III) complexes and the free ligands were evaluated against *S. epidermidis*, *S. aureus*, and *E. coli* using the agar diffusion method. The antimicrobial responses of the complexes and control samples against *S. epidermidis* and *S. aureus* are shown in Figures 9 and 10, respectively, while the corresponding inhibition zone diameters are summarized in Table 3.

Among the compounds tested, $Eu(btfa)_3(dmphen)$ exhibited the highest antimicrobial activity against all three bacterial species. As shown in Table 3, the starting materials $EuCl_3{\cdot}6H_2O$ and Hbtfa, as well as the DMF solvent control, produced little or no inhibition of bacterial growth when compared with the Eu(III) complexes and the dmphen ligand. The dmphen ligand itself displayed considerable antibacterial activity against both Gram-positive and Gram-negative bacteria. Ligands based on the 1,10-phenanthroline framework have been extensively investigated for their antimicrobial properties, both in their free form and when coordinated to metal ions (Liu et al., 2013; O'Shaughnessy et al., 2023). Numerous transition-metal complexes containing phenanthroline derivatives, including Cu(II), Zn(II), and Mn(II) complexes, have demonstrated significant antimicrobial activity. This behavior has frequently been attributed to the ability of the planar phenanthroline ligand to interact with DNA through π–π stacking interactions and intercalation between nucleic acid base pairs (Collins & Franzblau, 1997; Shahabadi et al., 2011). Given the structural similarity between dmphen and 1,10-phenanthroline, it is plausible that dmphen contributes to antimicrobial activity by interfering with DNA replication and transcription processes or by promoting DNA damage within microbial cells.

Chelation of hydrophobic ligands around the Eu(III) center reduces the effective charge density of the metal ion and generally increases the overall lipophilicity of the resulting coordination complex. Enhanced lipophilicity is expected to facilitate permeation of the complex through the lipid-rich cell membranes of microorganisms, thereby improving cellular uptake and increasing its ability to disrupt essential biological processes. The precursor complex $Eu(btfa)_3(H_2O)_2$ exhibited measurable antibacterial activity against all tested bacterial strains. However, upon replacement of the coordinated water molecules with the dmphen ligand to form $Eu(btfa)_3(dmphen)$, the inhibition zones increased by approximately 10 mm relative to those observed for $Eu(btfa)_3(H_2O)_2$.

The enhanced antimicrobial activity of $Eu(btfa)_3(dmphen)$ may arise from two complementary effects. First, coordination of the hydrophobic dmphen ligand increases the overall lipophilic character of the complex, potentially improving its penetration through bacterial cell membranes. Second, the coordinated dmphen ligand may actively participate in interactions with intracellular DNA, leading to disruption of vital cellular functions and inhibition of bacterial growth. The combined effects of improved cellular uptake and the biological activity of the phenanthroline-based ligand likely account for the superior antimicrobial performance of $Eu(btfa)_3(dmphen)$ compared with its aqua analogue.

To the best of our knowledge, this study represents the first report describing the antimicrobial activity of a lanthanide complex containing the coordinated ligand 2,9-dimethyl-1,10-

phenanthroline (dmphen). The results demonstrate that incorporation of dmphen into the coordination sphere of Eu(III) substantially enhances antibacterial activity, highlighting the potential of lanthanide–phenanthroline systems as promising candidates for the development of new antimicrobial agents.

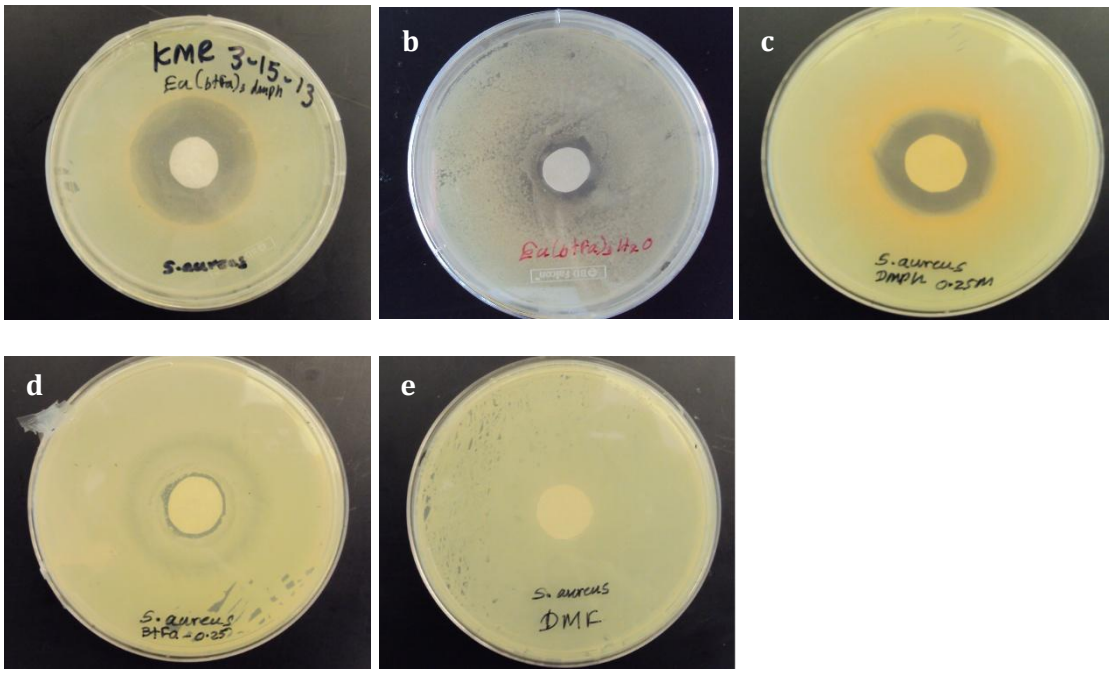

Figure 9. Antibacterial activity of 0.25 M (a) $Eu(btfa)_3$dmphen, (b) $Eu(btfa)_{3(}H_2O)_{2,}$ (c) dmphen, (d) btfa, and (e) N,N-dimethyl formamide (DMF) against *s. aureus*

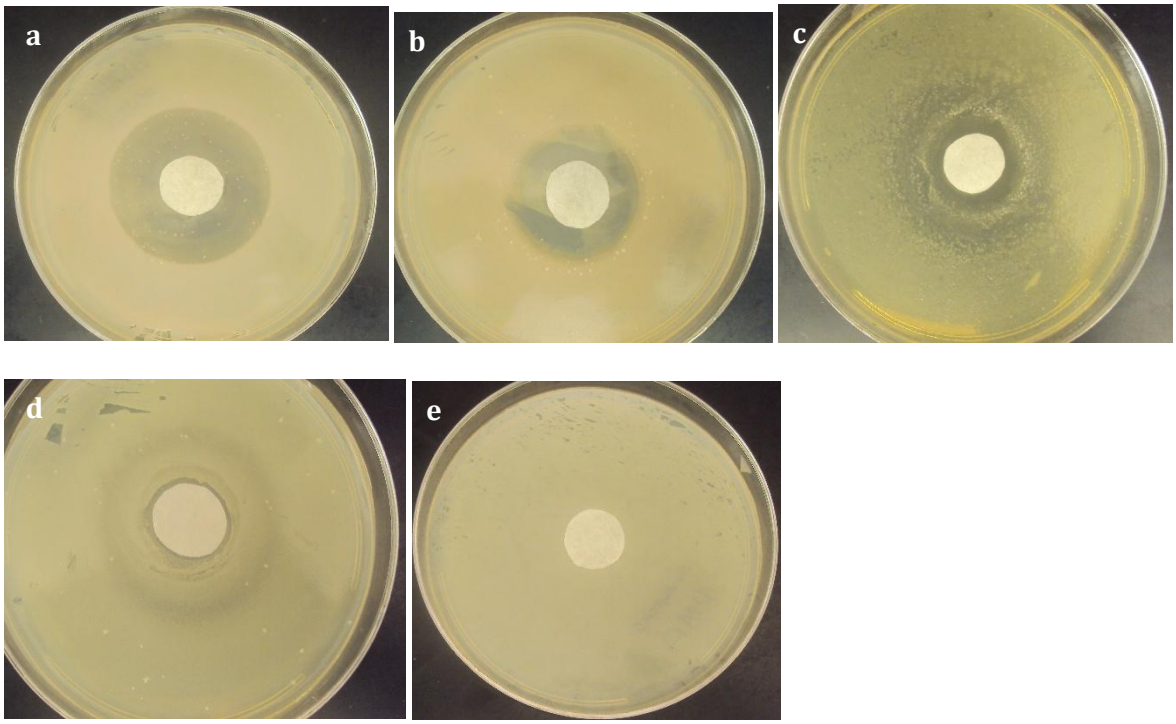

Figure 10. Antibacterial activity of 0.25 M (a) $Eu(btfa)_3$dmphen, (b) $Eu(btfa)_{3(}H_2O)_2$, (c) dmphen, (d) btfa, and (e) N,N-dimethyl formamide, against *S. epidermidis*

Table 3. Inhibition zones of the bacteria after incubating with the complexes and the ligands

Compounds	Inhibition zone (mm)											
	S. aureus			*SD ±*	*S. epidermidis*			*SD ±*	*E. coli*			*SD ±*
$Eu(btfa)_3dmph$	26	28	28	*1.1*	23	25	25	*1.1*	24	26	26	*1.1*
$Eu(btfa)_3(H_2O)_2$	18	16	18	*1.1*	16	17	16	*0.5*	16	16	17	*0.5*
Dmph-ligand	21	22	20	*1*	16	16	17	*0.5*	25	26	25	*0.5*
Btfa-ligand	7	6	6	*0.58*	3	4	4	*0.5*	26	28	28	*1.1*
DMF- solvent	0	0	0	*0*	0	0	0	*0*	0	0	0	*0*
$EuCl_3{\cdot}6H_2O$	0	0	0	*0*	0	0	0	*0*	0	0	0	*0*

Minimum inhibitory concentration studies

Alamar Blue has been widely employed in biomedical and microbiological research for evaluating the susceptibility of microorganisms to antimicrobial agents (Collins & Franzblau, 1997). Numerous studies have demonstrated its effectiveness as a rapid and reliable indicator for antimicrobial screening and determination of minimum inhibitory concentrations against a variety of bacterial pathogens. In the present study, the Alamar Blue assay was used to determine the MIC values of the synthesized Eu(III) complex. Compared with conventional plate-counting methods, the assay provides a simple visual means of assessing bacterial viability through a distinct color change from blue to pink, thereby facilitating rapid identification of inhibitory concentrations.

The Alamar Blue reagent functions by monitoring the metabolic activity of living cells. Its active component, resazurin, is a blue, non-fluorescent redox indicator that is reduced by metabolically active cells to form resorufin, a pink and highly fluorescent product (Page et al., 1993). During cellular respiration, the dye acts as an intermediate electron acceptor within the electron transport chain without disrupting normal electron-transfer processes. As viable bacterial cells continuously generate reducing equivalents, resazurin is converted to resorufin, resulting in a visible color change from blue to pink (Kadeřábková et al., 2024).

In wells containing metabolically active bacteria, the Alamar Blue reagent exhibited a pink coloration, indicating continued bacterial growth and viability. In contrast, wells that remained blue contained no detectable viable bacterial population, indicating effective inhibition of microbial growth. Thus, the MIC was defined as the lowest concentration of a compound that prevented the color change from blue to pink.

As illustrated in Figure 11, $Eu(btfa)_3(dmphen)$ displayed greater antimicrobial activity than $Eu(btfa)_3(H_2O)_2$. This enhanced activity is consistent with the larger inhibition zones observed in the agar diffusion studies. The MIC values determined for the Eu(III) complexes, and starting materials are summarized in Table 4. These results further confirm that coordination of the dmphen ligand significantly enhances the antimicrobial activity of the Eu(III) complex and highlight the potential of phenanthroline-based lanthanide complexes as promising antimicrobial agents.

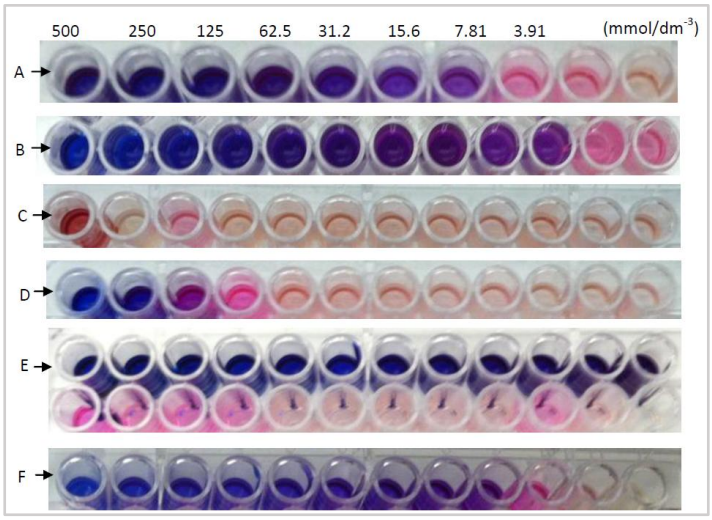

Figure 11. Alamar Blue assay used to determine the MIC of (A) 0.1 M btfa, (B) 0.1 M dmphen, (C) 0.1 M $EuCl_3 \cdot 6H_2O$, (D) N,N-Dimethyl Formamide (DMF), (E) 0.1 M $Eu(btfa)_3$dmphen complex and (F) 0.1 M $Eu(btfa)_3(H_2O)_2$ complex against *S. aureus*

Table 2: Minimum inhibitory concentration studies against *S. aureus*

Sample	**Minimum Inhibition Concentration** (mol dm^{-3})
$Eu(btfa)_3$dmph	5.9×10^{-5}
dmph	5.14×10^{-4}
$Eu(btfa)_3(H_2O)_2$	11.3×10^{-4}
$EuCl_3 \cdot 6H_2O$	No MIC
btfa	13.0×10^{-4}
DMF (Solvent)	9.98×10^{-50}

Conclusion

Here we have reported the synthesis and materials characterization of $Eu(btfa)_3$(dmphen) complex. The structure of the title complex was established by single crystal X-ray diffraction studies. The coordination sphere is a distorted square antiprism where the Eu(III) metal center is occupied by six oxygen atoms (from three btfa ligands) and two nitrogen atoms (from dmphen ligand). Both btfa and dmphen ligands are responsible for the light absorption of the complex. Upon ligand excitation, the title complex exhibits narrow red luminescence with a maximum emission intensity at 614 nm. The luminescent quantum yield and the lifetime values are greatly enhanced by the substitution of coordinated aqua ligands with the dmphen ligand. Both direct excitation and the ligand-based excitation of $Eu(btfa)_3$(dmphen) gave comparable luminescent lifetime values suggesting that the vibrational quenching of qua ligands may be responsible for lower quantum yield of the aqua complex. A synthetic method was developed to prepare biocompatible and highly luminescent Eu(btfa)3dmph complex-incorporated silica nanomaterials using modified Stöber method. The luminescent studies show that Eu(btfa)3dmph incorporated silica nanoparticles have intense luminescence at 614 nm. The higher luminescent quantum yield value was observed for the 40 mg Eu(btfa)3dmph incorporated silica nanoparticles (11.58%) compared to 20 mg and 30 mg Eu(btfa)3dmph incorporated silica nanoparticles (3.1%). The diameter of the nanoparticles was found to be in the range from 30 to

50 nm using SEM imaging. The Eu(btfa)3dmph incorporated silica nanomaterial is highly dispersible in water with potential biomedical imaging applications. These results confirm that the luminescence performance of the $Eu(btfa)_3$(dmphen)-incorporated silica nanoparticles is strongly dependent on the lanthanide complex concentration within the silica matrix, highlighting the importance of optimizing the doping level to achieve maximum emission efficiency. $Eu(btfa)_3$(dmphen) complex shows enhanced antimicrobial activity against *S. epidermidis*, *S. aureus*, and *E. coli* bacteria species. The improved antimicrobial activity of the title complex may be due to the presence of hydrophobic dmphen ligand which can interact with DNA molecules within the bacterial cells.

Acknowledgments

The research work is supported by the Faculty Start-up Funds, Undergraduate Academic Project Grant Program, and Summer Research Assistantship at the Western Carolina University

Declaration of Funding Sources

This research did not receive any specific grant from funding agencies in the public, commercial, or not-for-profit sectors.

Conflict of interest statement

The authors declare no conflict of interest.

References

Campello, M. P. C., Palma, E., Correia, I., Paulo, P. M. R., Matos, A., Rino, J., Coimbra, J., Pessoa, J. C., Gambino, D., Paulo, A., & Marques, F. (2019). Lanthanide complexes with phenanthroline-based ligands: Insights into cell death mechanisms obtained by microscopy techniques. *Dalton Transactions*, *48*(14), 4611–4624. https://doi.org/10.1039/c9dt00640k

Collins, L. A., & Franzblau, S. G. (1997). Microplate Alamar Blue assay versus BACTEC 460 system for high-throughput screening of compounds against Mycobacterium tuberculosis and Mycobacterium avium. *Antimicrobial Agents and Chemotherapy*, *41*(5), 1004–1009. https://doi.org/10.1128/aac.41.5.1004

Dalal, A., Nehra, K., Hooda, A., Singh, D., Kumar, P., Kumar, S., Malik, R. S., & Rathi, B. (2023). Luminous lanthanide diketonates: Review on synthesis and optoelectronic characterizations. *Inorganica Chimica Acta*, *550*, Article 121406. https://doi.org/10.1016/j.ica.2023.121406

De Silva, C. R., Maeyer, J. R., Wang, R., Nichol, G. S., & Zheng, Z. (2007). Adducts of europium β-diketonates with nitrogen p,p′-disubstituted bipyridine and phenanthroline ligands: Synthesis, structural characterization, and luminescence studies. *Inorganica Chimica Acta*, *360*, 3543–3552. https://doi.org/10.1016/j.ica.2007.04.049

Galaup, C., Azéma, J., Tisnès, P., Picard, C., Ramos, P., Juanes, O., Brunet, E., & Rodríguez-Ubis, J. C. (2002). Luminescence of Eu^{3+} and Tb^{3+} complexes of two macrobicyclic ligands derived from a tetralactam ring and a chromophoric antenna. *Helvetica Chimica Acta*, *85*(6), 1613–1625.

Gao, S., Huang, M., Sun, Z., Li, D., Xie, C., Feng, L., Liu, S., Zheng, K., & Pang, Q. (2021). A new mixed-ligand lanthanum(III) complex with salicylic acid and 1,10-phenanthroline: Synthesis, characterization, antibacterial activity, and underlying mechanism. *Journal of*

Molecular Structure, *1225*, Article 129096. https://doi.org/10.1016/j.molstruc.2020.129096

Görller-Walrand, C., & Binnemans, K. (1998). Spectral intensities of f–f transitions. In K. A. Gschneidner Jr. & L. Eyring (Eds.), *Handbook on the physics and chemistry of rare earths* (Vol. 25, pp. 101–264). Elsevier. https://doi.org/10.1016/S0168-1273(98)25006-9

Junker, A. K. R., Hill, L. R., Thompson, A. L., Faulkner, S., & Sørensen, T. J. (2018). Shining light on the antenna chromophore in lanthanide-based dyes. *Dalton Transactions*, *47*(14), 4794–4803. https://doi.org/10.1039/c7dt04788f

Kadeřábková, N., Mahmood, A. J. S., & Mavridou, D. A. I. (2024). Antibiotic susceptibility testing using minimum inhibitory concentration (MIC) assays. *Antimicrobials & Resistance*, *2*, Article 37. https://doi.org/10.1038/s44259-024-00051-6

Liu, J., Ren, N., Zhang, J., & Zhang, C. (2013). Preparation, thermodynamic property and antimicrobial activity of some rare-earth(III) complexes with 3-bromo-5-iodobenzoic acid and 1,10-phenanthroline. *Thermochimica Acta*, *570*, 51–58. https://doi.org/10.1016/j.tca.2013.07.020

Ma, H., Liu, Q., Akam-Baxter, E. A., Huang, Y., Yuan, J., Huang, H., Liu, D., & Song, B. (2025). Lanthanide complexes-doped silica nanoparticles for dual-modal ratiometric time-gated luminescence/magnetic resonance imaging of inflammatory diseases. *Analytical Chemistry*, *97*(23), 12108–12115. https://doi.org/10.1021/acs.analchem.5c00455

Nihonyanagi, S., & Kanemitsu, Y. (2004). Enhanced luminescence from electron–hole droplets in silicon nanolayers. *Applied Physics Letters*, *85*(23), 5721–5723. https://doi.org/10.1063/1.1829161

O'Shaughnessy, M., Hurley, J., Dillon, S. C., Herra, C., McCarron, P., McCann, M., Devereux, M., & Howe, O. (2023). Antibacterial activity of metal–phenanthroline complexes against multidrug-resistant Irish clinical isolates: A whole genome sequencing approach. *Journal of Biological Inorganic Chemistry*, *28*(2), 153–171. https://doi.org/10.1007/s00775-022-01979-8

Page, B., Page, M., & Noel, C. (1993). A new fluorometric assay for cytotoxicity measurements in vitro. *International Journal of Oncology*, *3*(3), 473–476. https://doi.org/10.3892/IJO.3.3.473

Santra, S., Khasanov, A. F., Mukherjee, A., Rahman, M., Kovalev, I. S., Kopchuk, D. S., Zyryanov, G. V., Majee, A., Chupakhin, O. N., & Charushin, V. N. (2018). Mono- and polyazatriphenylene-based ligands: An updated library of synthetic strategies (2001–2018). *European Journal of Organic Chemistry*, *2018*(33–34), 4351–4375. https://doi.org/10.1002/ejoc.201800635

Shahabadi, N., Mohammadi, S., & Alizadeh, R. (2011). DNA interaction studies of a new platinum(II) complex containing different aromatic dinitrogen ligands. *Bioinorganic Chemistry and Applications*, *2011*, Article 429241. https://doi.org/10.1155/2011/429241

Singla, M. L., Muhamed, S. M., & Kumar, M. (2009). Optical characterization of ZnO nanoparticles capped with various surfactants. *Journal of Luminescence*, *129*(5), 434–438. https://doi.org/10.1016/j.jlumin.2008.11.021

Tan, M., Wang, G., Hai, X., Ye, Z., & Yuan, J. J. (2004). Development of functionalized fluorescent europium nanoparticles for biolabeling and time-resolved fluorometric applications. *Journal of Materials Chemistry*, *14*(19), 2896–2901. https://doi.org/10.1039/b407535h

Tessitore, G., Mandl, G. A., Maurizio, S. L., Kaur, M., & Capobianco, J. A. (2023). The role of lanthanide luminescence in advancing technology. *RSC Advances*, *13*(26), 17787–17811. https://doi.org/10.1039/d3ra00991b